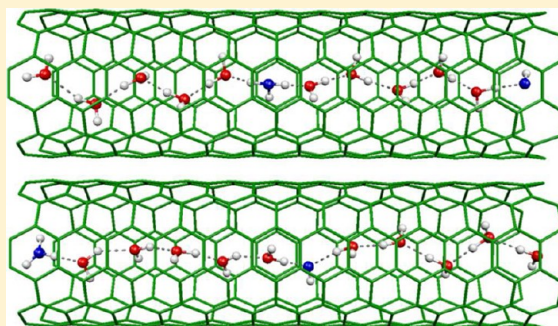


Hydroxide Ion Can Move Faster Than an Excess Proton through One-Dimensional Water Chains in Hydrophobic Narrow Pores

Arindam Bankura[†] and Amalendu Chandra*

Department of Chemistry, Indian Institute of Technology, Kanpur, India 208016

ABSTRACT: Carbon nanotubes (CNT) are known to provide a hydrophobic, confined environment for water where its structure and dynamics can be very different from those of bulk water. In particular, narrow CNTs of the type (6,6) allow only a single one-dimensional (1D) chain of water molecules inside them, thus providing an idealized scenario to study motion in 1D along water chains. In the present study, we have investigated structural and dynamic behavior of water and also of an excess proton and hydroxide ion in water-filled narrow CNTs by means of ab initio molecular dynamics and combined quantum-classical simulations. The main focus of the present work is on the molecular mechanism and kinetics of hydronium and hydroxide ion migration along 1D water chains of different lengths in confinement. It is found that the hydrogen-bonded structures of water and the excess proton and hydroxide ion in CNTs can be very different from those in bulk, and these altered solvation structures play critical roles in determining the proton-transfer (PT) rates along water chains. For the present 1D chain systems, the hydroxide ion is found to migrate at a slightly faster rate than the excess proton, unlike their relative mobilities in bulk water. This faster migration of the hydroxide ion is found not only in CNTs with periodicity along the tube axis but also in isolated CNTs where the excess proton and the hydroxide ion are allowed to move under the influence of an electric field of an oppositely charged ion. The roles of rotational jumps and hydrogen-bond fluctuations in the PT events are discussed. In addition, the significance of hydrogen-bonding defects on the dynamics of an excess proton and hydroxide ion is also discussed for varying chain lengths.



1. INTRODUCTION

Proton transfer in aqueous systems in confinement occurs in many chemical and biological systems.^{1–6} For example, passage of protons through narrow ion channels containing water molecules in their interior region involves proton transfer (PT) through water chains. Ion channels are usually formed by integral membrane proteins, and their diameters are such that the permeation process involves single-file movement of partially dehydrated ions and water molecules through the interior of the pores. Proton transfer through membranes is a fundamental issue in ATP synthesis and also in the generation of electrical power in hydrogen fuel cells.^{7–9} Since these systems possess structural inhomogeneity at their interior surfaces, including charges, the structural and dynamic behavior of water and proton transport kinetics in these systems are determined by combined effects of confinement and interactions with inhomogeneously distributed atomistic structures of the surfaces, including Coulomb interactions with the surface charges. In this respect, carbon nanotubes (CNTs) offer a remarkably simple model system where the translocation of protons along a one-dimensional (1D) hydrogen-bonded chain of water molecules in confinement can be studied quantitatively in the absence of any surface inhomogeneity and specific interactions with interior surface sites. By probing the encapsulation-induced changes in water, a series of recent experimental studies have demonstrated that water can enter carbon nanotubes at room temperature.^{10–19}

The incorporation of water into CNTs has also been demonstrated by several recent theoretical studies.^{20–29} By employing classical molecular dynamics simulations, Hummer and co-workers^{20,21} have shown that water spontaneously fills the hydrophobic channel of CNTs with periodic transitions between filled and empty states. Simulations of water-filled (6,6) single-wall CNTs have shown that water forms a 1D hydrogen-bonded ordered chain inside the nanotube.^{20–28} The smooth interior cavity surface of the (6,6) CNT forces the water chain to maintain a quasilinear geometry where each water molecule donates one hydrogen bond and accepts one. Recently, Mukherjee et al.²⁵ have shown that water reorientation inside the CNTs occurs through large-amplitude angular jumps in which the hydrogen atom participating in the hydrogen bond and the free hydrogen atom of the same water repeatedly exchange their positions. Computer simulations of an excess proton in a small, isolated water-chain system^{30–35} have shown that the excess charge prefers to stay at the center of the water chain since the hydronium ion is effectively repelled by the end points of the water chain. The hydronium ion mobility in CNTs with periodicity has also been studied using the multistate empirical valence-bond (MS-EVB) model^{35–37} and ab initio molecular dynamics.^{35,38} These

Received: February 14, 2012

Revised: July 2, 2012

Published: July 13, 2012

simulations have shown that 1D chains of hydrogen-bonded water molecules are very good proton conductors. Proton conduction in water-filled CNTs under external electric fields and also through more structured pores of biomolecules and functionalized CNTs has also been studied in recent years.^{39–46} The rate of proton diffusion in water is generally very high because the mechanism of proton transport does not require the net molecular displacement of the ionic solute or water molecules along the diffusion pathway; rather the protons can hop through the hydrogen-bonded network via the “Grotthuss” mechanism,^{47,48} involving structural rearrangement. It has been reported that the rate of hydronium ion mobility in CNTs is much faster than that of the bulk.³⁵ However, no such study is available for hydroxide ion mobility in CNTs. The structural diffusion of a hydrated excess proton (i.e., hydronium ion) and the one with one fewer proton (i.e., the hydroxide ion) in bulk aqueous solutions has been studied in great detail through dynamic simulations in recent years.^{48–57} These studies have unearthed various molecular details of the proton-transfer mechanism and the role of hydrogen-bond fluctuations in these three-dimensional (3D) systems. The faster proton-transfer (PT) rate in CNT³⁵ is likely to arise from a mechanism different from that in bulk aqueous solutions. Because of this high PT rate, water-filled carbon nanotubes are expected to play an important role in future nanoscale devices for proton storage and transport applications. Hence, an in-depth study of the structure and dynamics of water wires in narrow CNTs and proton transport through such wires would certainly be a worthwhile exercise.

In this paper, we present the results of dynamic simulations of 1D water chains with protonic defects, such as an excess proton and a hydroxide ion, encapsulated inside narrow single-wall (6,6) CNTs of varying length. The smallest systems are studied by *ab initio* molecular dynamics.⁵⁸ However, as the chain length is increased, the number of water and carbon atoms increases significantly, and the computational cost for these larger systems becomes very high for full *ab initio* molecular dynamic simulations. Hence, in order to study migration of an excess proton and a hydroxide ion in longer chains, we have employed the method of combined quantum-classical (QM/MM) simulations,^{59,60} where the chemically active part is treated by quantum chemical methods (QM), and the rest of the system is assumed to be chemically inert and treated by molecular mechanics or classical force fields (MM). In the present work, such hybrid QM/MM molecular dynamic simulations are carried out by treating all water molecules and protonic defects quantum mechanically and the carbon atoms of CNTs classically. We note that the protonic defects (i.e., the excess proton and hydroxide ion) migrate through hydrogen-bonded water chains via PT processes, where the carbon atoms do not play any active role other than providing the confined environment.

We have studied systems of different chain lengths since an increase in chain length reduces the effects of hydrogen-bonding defects that are usually created at the boundaries due to periodic boundary conditions. At the boundaries, chains of opposite orientations meet, and this can lead to two types of orientational defects with different hydrogen-bonding environments. Such defects can also arise due to thermal fluctuations in a normal chain without any periodic boundary conditions. A D defect arises when a water molecule accepts two hydrogen bonds and donates none, whereas an L defect occurs when a water molecule donates two hydrogen bonds and accepts none

(Figure 1). Previous studies on the migration of an excess proton through water chains have shown that the rate of PT

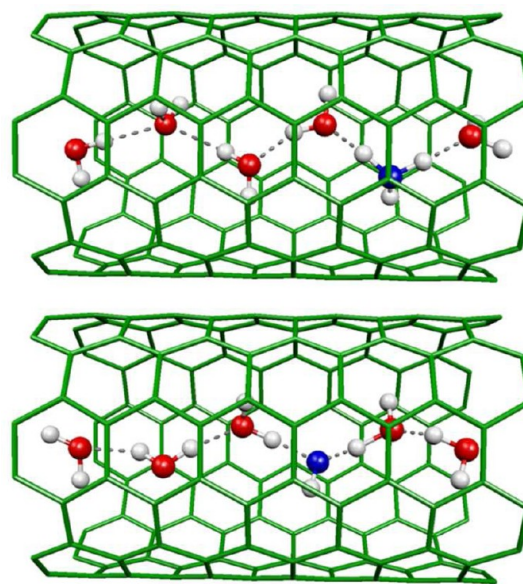


Figure 1. Snapshots taken from *ab initio* molecular-dynamic simulation trajectories of hydrogen-bonded chains of water molecules ($N = 6$) containing an excess proton and a D defect (top) and a hydroxide ion and an L defect (bottom). The hydronium and hydroxyl oxygens are shown in blue.

can be reduced by these defects because they break the favorable hydrogen-bonded environment required for proton movement.³⁵ In the present work, we have performed a detailed study of the dynamics of these defects and their roles in proton-transfer processes for cases of both hydronium and hydroxide ions. We have investigated the rates and mechanism of proton migration and how these properties change with increasing chain length. In particular, the roles of hydrogen-bond fluctuations and rotational jumps in PT in these narrow pores are investigated in great detail.

The rest of the paper is organized as follows. The simulation methods and other computational details are presented in Section 2. The solvation structure, hydrogen-bond properties, rotational dynamics, and angular jumps of water molecules inside CNTs are described in Section 3. In Section 4, the hydration structures, rates, and mechanisms of PT through water chains containing H^+ and OH^- ions in CNTs are presented. In Section 5, PT in isolated chains in the presence of external fields created by the presence of counterions is discussed. Our conclusions are then briefly summarized.

2. METHODOLOGY AND COMPUTATIONAL DETAILS

We have considered single-wall (6,6) CNTs of four different lengths. In order to determine the number (N) of water molecules that fill up these nanotubes under ambient conditions, we first carried out several classical molecular dynamic simulations with the nanotubes immersed in a large bath of SPC/E water.⁶¹ Our classical simulations as well as previous studies^{20,35,38} have shown that only one water molecule is commensurate with the length of one unit cell of (6,6) CNT. We carried out molecular dynamics simulations with 6, 12, 18, and 30 water molecules confined in (6,6) armchair-type single-wall CNTs of lengths, L , equal to 15.1,

29.1, 43.6, and 72.7 Å comprising 144, 288, 432, and 720 carbon atoms, respectively. In order to study the structural and dynamic behavior of protonic defect systems, we replaced one water molecule by a hydronium ion or a hydroxide ion. The systems were kept in the central region of an orthorhombic box of length 13.5 Å in *x*- and *y*-directions, whereas the length of the box was taken to be the same as that of CNT along the *z*-direction. All systems were first equilibrated for 10 ns through classical simulations, employing a periodic boundary condition along the axis of carbon nanotubes, and then these systems were subjected to ab initio molecular dynamics (AIMD) (for *L* = 15.1 Å only) and QM/MM (all lengths) simulations. In order to study the properties of pure water in confined nanotube systems, we also carried out an AIMD simulation with six water molecules in a CNT of 15.1 Å length and another QM/MM simulation with 12 water molecules in a CNT of 29.1 Å length, with periodicity along the tube axis but without any protonic defects.

The ab initio simulations of the smallest chain systems (*N* = 6) were carried out using the Car–Parrinello molecular dynamics method⁵⁸ and the CPMD code.⁶² In these simulations, all atoms of the systems, including the carbon atoms of CNTs, were treated quantum mechanically, and the interatomic forces were calculated “on the fly”, at each time step, from electronic structure calculations based on density functional theory (DFT).⁶³ We employed the BLYP density functional⁶⁴ in the present DFT calculations. The core electrons of all the atoms were treated by Vanderbilt ultrasoft pseudopotentials,⁶⁵ and the plane wave expansions of the valence-electron wave functions were truncated at a kinetic energy of 25 Ry. The simulations were carried out with a time step of 5 au and a fictitious electronic orbital mass of 800 au. In order to reduce the importance of quantum effects, all hydrogen atoms of water molecules were given the mass of deuterium. However, we will continue to refer to the simulated species as H⁺, OH[−], and H₂O for convenience. As described above, the initial configurations of all the systems were first generated from classical molecular dynamic simulations. Subsequently, we equilibrated all of these systems for about 10 ps in an NVT ensemble at 300 K using the Nose–Hoover chain method,⁶⁶ and thereafter, we continued the runs in the NVE ensemble for another 25 ps for calculations of various structural and dynamic quantities. We note that our choice of deuterium mass for hydrogen atoms ensured that electronic adiabaticity and energy conservation were maintained throughout the simulations for the chosen values of the fictitious electronic mass parameter and time step. The choice of a proper value of the electronic mass parameter is an important issue in performing Car–Parrinello simulations in the right manner. While a value of 800 au was shown not to be reliable for H₂O⁶⁷ for maintaining electronic adiabaticity, it was found to be acceptable for the present systems because no significant drift of the electronic kinetic energy was observed during the entire simulation process due to the use of heavier deuterium atoms in place of hydrogens.

In addition to employing the ab initio molecular dynamics method for simulating *N* = 6 systems in confinement, we also employed the QM/MM method^{59,60} to study larger systems (*N* = 12, 18, 30 and also *N* = 6) by partitioning each entire system into quantum water (including H⁺/OH[−]) and classical CNT parts. The QM part was calculated using CPMD while the MM part was treated using the GROMOS96 force field.⁶⁸ In general, the QM atoms interact with the MM ones through electrostatic,

van der Waals, and bonded interactions. In the present simulations, the MM part consists of carbon atoms which are considered as static van der Waals atoms without any partial charges. Hence, the electrostatic and bonded interactions between QM and MM parts are absent in the present systems, and we needed to consider only the nonbonded short-range van der Waals interaction between atoms of these parts. The parameters of such van der Waals interactions were taken from the Amber force field of interactions.⁶⁹ By using the above scheme, we performed a number of QM/MM simulations of water chains of different lengths, both with and without protonic defects, in confinement of narrow CNTs. The positions of CNT carbon atoms were kept fixed at their equilibrium positions during these QM/MM calculations. Initially, each system was equilibrated in an NVT ensemble at 300 K for 10 ps, and subsequently, simulations of each system were continued for at least another 40–60 ps in an NVE ensemble. The details of all the systems studied in this work are given in Table 1.

Table 1. Details of Systems Simulated in the Present Work^a

system	method	<i>N</i>	<i>N_c</i>	<i>L</i> (Å)	H ⁺ /OH [−] / H ₂ O	simulation period (ps)
1a	CPMD	6	144	15.1	H ⁺ /H ₂ O	25
2a	QM/ MM	6	144	15.1	H ⁺ /H ₂ O	40
3a	QM/ MM	12	288	29.1	H ⁺ /H ₂ O	40
4a	QM/ MM	18	432	43.6	H ⁺ /H ₂ O	40
5a	QM/ MM	30	720	72.7	H ⁺ /H ₂ O	40
1b	CPMD	6	144	15.1	OH [−] /H ₂ O	25
2b	QM/ MM	6	144	15.1	OH [−] /H ₂ O	40
3b	QM/ MM	12	288	29.1	OH [−] /H ₂ O	40
4b	QM/ MM	18	432	43.6	OH [−] /H ₂ O	40
5b	QM/ MM	30	720	72.7	OH [−] /H ₂ O	40
6	CPMD	6	144	15.1	H ₂ O	40
7	QM/ MM	12	288	29.1	H ₂ O	60

^aThe numbers of oxygen (*N*) and carbon atoms (*N_c*), box length in *z*-direction (*L*), and total simulation periods are given. Also included is information on the method employed in the simulations (CPMD or QM/MM) and the nature of the protonic defect (H⁺ or OH[−] or pure water).

3. PROPERTIES OF PURE WATER CONFINED IN (6,6) CARBON NANOTUBES

In the bulk phase, water molecules form a 3D tetrahedral hydrogen-bonded network with each water forming nearly four hydrogen bonds. In a narrow CNT which can support only a single-file water chain inside, each water molecule loses on average two of its four hydrogen bonds. Now, each water molecule donates one hydrogen bond through one of its hydrogens and accepts one through its oxygen, thus producing an orientationally ordered 1D hydrogen-bonded chain inside the nanotube. For example, the average orientation of water dipoles with respect to the nanotube axis is found to be about 35°, which means that the water molecules are orientationally

ordered with their dipoles aligned more along the tube axis than in the directions perpendicular to it.

3.1. Hydrogen-Bond Dynamics of Confined Water.

Studies of hydrogen-bond dynamics are extremely important in understanding the origin of many fascinating dynamic features of water in varying environments. Here, we present our calculations of hydrogen-bond dynamics in the confined water systems. We have used a set of geometric criteria for defining hydrogen bonds where two water molecules are taken to be hydrogen-bonded if their inter-oxygen distance is less than 3.5 Å and the hydrogen–oxygen distance is less than 2.45 Å, simultaneously. We have computed the dynamics of hydrogen bonds by using the population-correlation-function approach.^{70–73} In particular, we have calculated the so-called continuous hydrogen-bond correlation function which describes the probability that a water pair, which was hydrogen-bonded at $t = 0$, remains continuously bonded up to time t . The integral of this correlation function describes the average lifetime (τ_{HB}) of a hydrogen bond between two water molecules inside the CNT.

We have obtained a value of 18.5 ps by integrating the time decay of the continuous hydrogen-bond correlation function for the pure water system ($N = 12$) in the CNT. The timescale of the hydrogen-bond relaxation of water–water pairs in the smaller system ($N = 6$) is also found to be rather similar. We note that this hydrogen-bond lifetime of water in the confined 1D chain is much longer than that in bulk water, which has been reported to be about 2 ps from ab initio simulations.^{55,74,75} This slower hydrogen-bond dynamic can be attributed to more compact hydrogen bonding inside the CNT, which supports much less cooperativity and allows much less fluctuation. This timescale of hydrogen-bond dynamics also reveals that, even under extreme confinement, breaking and reformation of hydrogen bonds can still occur, although much less frequently than they do in liquid water at room temperature.

3.2. Orientational Relaxation of Confined Water Molecules. Rotational motion of water molecules is known to play a primary role in the breaking of hydrogen bonds. Hence, in view of slower hydrogen-bond dynamics discussed in the previous subsection, it is worthwhile to see to what extent the rotational motion of water molecules in confined chain is altered from that in bulk water. The rotational motion of water molecules is analyzed by calculating the orientational time-correlation function, $C_l^\alpha(t)$, defined by

$$C_l^\alpha(t) = \frac{\langle P_l[e^\alpha(t) \cdot e^\alpha(0)] \rangle}{\langle P_l[e^\alpha(0) \cdot e^\alpha(0)] \rangle} \quad (1)$$

where P_l is the Legendre polynomial of rank l and e^α can be any vector joining two points on the water molecule. The reorientation time, τ_l , can be obtained by integrating the corresponding l th-order correlation function. The ratio of the first two orientational relaxation times should be equal to three if the relaxation is Debye-like.⁷⁶ Deviations occur if the relaxation involves nondiffusive processes. We have calculated τ_1 and τ_2 for the reorientational relaxation of the molecular dipoles and also of OH and HH vectors of the confined water molecules.

The rotational motion of water dipoles in confined 1D chains is found to be very slow due to the more rigid hydrogen-bonded environment compared with that of bulk water. The correlation function of the dipole vectors, $C_l^\mu(t)$, shows a short

time decay ($\tau_1^{\text{fast}} \sim 61$ fs, $\tau_2^{\text{fast}} \sim 50$ fs) followed by a slow, long time decay ($\tau_1^{\text{slow}} \sim 1.6$ ns, $\tau_2^{\text{slow}} \sim 0.3$ ns). In fact, the long time rotational relaxation of the dipole vectors is extremely slow and their timescales may not be properly captured in our short simulations. The rotational correlation of the OH vectors, $C_l^{\text{OH}}(t)$, exhibits a rather rapid initial decay ($\tau_1^{\text{fast}} \sim 160$ fs, $\tau_2^{\text{fast}} \sim 60$ fs), followed by a slower decay ($\tau_1^{\text{slow}} \sim 7.4$ ps, $\tau_2^{\text{slow}} \sim 5.27$ ps). The rotational relaxation of the HH vectors is found to be relatively faster, and the corresponding timescales are $\tau_1^{\text{fast}} \sim 180$ fs, $\tau_1^{\text{slow}} \sim 3.9$ ps, $\tau_2^{\text{fast}} \sim 70$ fs, and $\tau_2^{\text{slow}} \sim 1.9$ ps. The ratio of the timescales of the first- and second-order reorientational correlation functions significantly deviates from three, which means that water rotation in narrow CNTs involves non-diffusive processes like angular jumps and not full Debye-like diffusion of incremental rotational steps. The issue of angular jumps is discussed in more detail below.

3.3. Rotational Jumps of Confined Water Molecules in Carbon Nanotubes. Recent simulations of liquid water⁷⁷ have shown that water reorientation occurs through large-amplitude angular jumps rather than through a sequence of small-amplitude angular diffusive steps. Therefore, it would be interesting to see how this angular-jump mechanism is changed as a result of confinement. Mukherjee et al.²⁵ studied the reorientational dynamics of water molecules inside the CNTs by classical molecular dynamic simulations using SPC/E,⁶¹ TIP3P,⁷⁸ and TIP5P⁷⁹ models. They found that the confined water molecules rotationally relax by an angular-jump mechanism in which a hydrogen atom of water, participating in the hydrogen bond, and the free hydrogen atom of the same water repeatedly exchange their positions. In our ab initio and QM/MM molecular dynamic simulations, we have also found angular jumps at the instant of hydrogen-bond breaking. Such an angular-jump event is shown in Figure 2 where the rotating water molecule is denoted as O*H1*H2*, and the oxygen of the neighboring water molecule, which accepts a hydrogen bond, is denoted as O'. The identity of the hydrogen-bonded hydrogen atom changes in the angular-jump process. In order

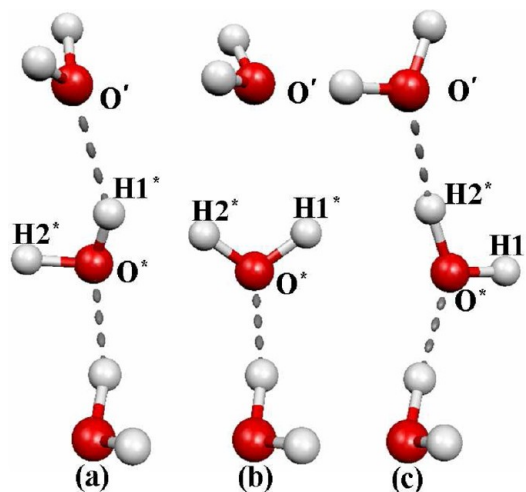


Figure 2. Different steps in the large-amplitude angular-jump mechanism of confined water molecules. The frames are taken from snapshots of a successful jump event in the simulation for $N = 12$. The water molecule O*H1*H2* is performing the angular jump. Initially, (a) H1* is hydrogen-bonded to the oxygen (O'), and H2* is free. After the angular jump, (c) H2* becomes hydrogen-bonded, and H1* is now free.

to investigate the angular jumps for a water molecule at time instant t , we first determined which hydrogen atom ($H1^*$ or $H2^*$) of that molecule participates in the hydrogen bonding with the oxygen (O') of a neighboring water. We defined two functions, $f_{H1}(t)$ and $f_{H2}(t)$, where $f_{H1}(t)$ is unity when the $H1^*$ atom participates in hydrogen bonding with O' according to the adopted definition and is zero otherwise, and $f_{H2}(t)$ is also defined in a similar way for the $H2^*$ atom. For each water molecule in the chain, we have computed these two functions. As described in ref 25, if the $H1^*$ atom is hydrogen-bonded and $H2^*$ is free then an angular jump would make $H2^*$ hydrogen-bonded and $H1^*$ free. Then, after the next jump, $H1^*$ becomes hydrogen-bonded and $H2^*$ is free. So, for a successful jump to take place for a given water molecule, $f_{H1}(t)$ goes from one to zero and $f_{H2}(t)$ goes from zero to one at a later instant, or vice versa. If $f_{H1}(t)$ goes from one to zero and back to one but $f_{H2}(t)$ remains zero throughout, or vice versa, it is not considered a successful jump. The starting and ending points of a jump event, t_1 and t_2 , respectively, are found from the points of the sudden changes of the slope of the angle versus time curves. We have calculated the time required to complete a successful jump from the difference between the starting time, t_1 , and the ending time, t_2 , of each jump event. The difference between the angle $\theta_{O'O^*H1^*}$ (or $\theta_{O'O^*H2^*}$) at t_1 and t_2 is the angle rotated by the water molecules during the rotational-jump process. In the angular-jump mechanism shown in Figure 2, the time step at which the difference between angles $\theta_{O'O^*H1^*}$ and $\theta_{O'O^*H2^*}$ is zero is denoted as the midpoint of the rotational angular-jump process. Considering this time to be $t = 0$, we have calculated the distances, $r_{H1^*O'}$, $r_{H2^*O'}$, $r_{O'O'}$, and angles, $\theta_{O'O^*H1^*}$ and $\theta_{O'O^*H2^*}$, over time windows of ± 250 fs. The corresponding average results are shown in Figure 3. From the

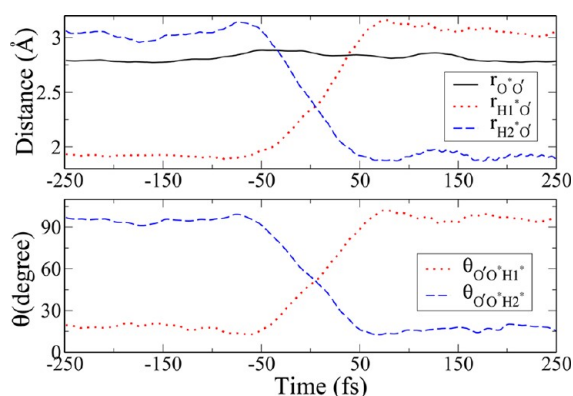


Figure 3. Time evolution of various distances and angles (as defined in the text) during the rotational jumps. The results of this figure were obtained by averaging over several successful jumps in the 1D chain with $N = 12$.

top panel of Figure 3, it is seen that the distance between the oxygen atoms ($r_{O'O'}$) remains almost constant, whereas the distance of $H1^*$ and $H2^*$ from O' ($r_{H1^*O'}$ and $r_{H2^*O'}$) changes during the angular-jump events. The changes of the angles $\theta_{O'O^*H1^*}$ and $\theta_{O'O^*H2^*}$ during the angular jump are shown in the bottom panel of Figure 3. The average jump amplitude is found to be about 90° . The average time required to complete a successful jump is found to be about 110 fs with a long tail up to 175 fs for the corresponding distribution. This average jump time is approximately comparable with the faster timescales of the rotational relaxation of the molecular vectors discussed in

Section 3.2. The average jump waiting time (the time difference between two such jumps in a particular water molecule) of a water molecule in the confined narrow nanotube system is found to be very slow, approximately 18 ps. This mean jump waiting time is comparable to our calculated average lifetime of hydrogen bonds discussed in Section 3.1. Thus, the hydrogen-bond lifetime captures the hydrogen-bond breaking dynamics due to the successful angular jumps. We may also note here that hydrogen-bond fluctuations due to unsuccessful jumps may also contribute to the hydrogen-bond breaking dynamics, hence HB lifetimes, when angular cutoffs are also used in addition to the distance cutoffs used here. We also note that this angular-jump mechanism and jump timescales exhibit characteristics qualitatively similar to those obtained in the classical simulation studies of ref 25.

4. EXCESS PROTON AND HYDROXIDE ION IN WATER-FILLED CARBON NANOTUBES

In this section, we study solvation and migration dynamics of an excess proton and a hydroxide ion through 1D hydrogen-bonded chains of water molecules. In these systems, the index of the oxygen of hydronium or hydroxide ion, denoted as O^* , changes due to PT events. The frequency of change of the O^* index provides information on how fast PT occurs in these systems. In general, we observe that the PT occurs very fast in these systems which means that the confinement provides a favorable hydrogen-bonded pathway for PT. Since the mechanism of PT is intimately linked to the solvation structure of the hydronium and hydroxide ions, we first discuss the hydrogen-bonded coordination of these ionic species in their first solvation shells.

4.1. Solvation Structure of Protonic Defects. The solvation structure of the hydronium ion is investigated by calculating the number of hydrogen bonds donated (N_{HB}^*) through its hydrogens while that of OH^- is studied by calculating the number of hydrogen bonds accepted (N_{HB}^{δ}) by it. It is found that the hydronium ion always donates two hydrogen bonds through its two hydrogens, and its third hydrogen remains free. The hydroxide ion, on the other hand, accepts two hydrogen bonds from the neighboring water molecules, and the hydroxyl hydrogen remains free all the time. Thus, in these water-filled narrow carbon nanotubes, both the hydronium and hydroxide ions stay in two-coordinated states.

During a PT process, the protonic defect (the hydronium or hydroxide ion) moves from one oxygen to another oxygen through a $O^* \cdots H \cdots O^\dagger$ bond, and this can be called a PT reaction pathway where O^\dagger denotes the oxygen where defects move after PT events. We calculate the difference between the two distances

$$\delta = d_{O^*H} - d_{O^\dagger H} \quad (2)$$

for each configuration, where δ is the associated asymmetric stretch and is chosen as the PT reaction coordinate.^{53,54} Small and large values of δ mean different solvation structures of the protonic defect during the PT process. When the value of δ is large, the protonic defect stays with one of the water molecules, and a small value of δ means that the proton is equally shared ($H_5O_2^+$ or $H_3O_2^-$) between two oxygen atoms. We first examine the free energy profiles for the PT reactions by calculating the probability distribution function, $P(\delta)$, from the simulation trajectories, and then we obtain the free energy profiles by using the following relation:

$$F(\delta) = -k_B T \ln P(\delta) \quad (3)$$

The free energy profiles obtained for the excess proton and hydroxide ion systems ($N = 12$) are shown in Figure 4. These

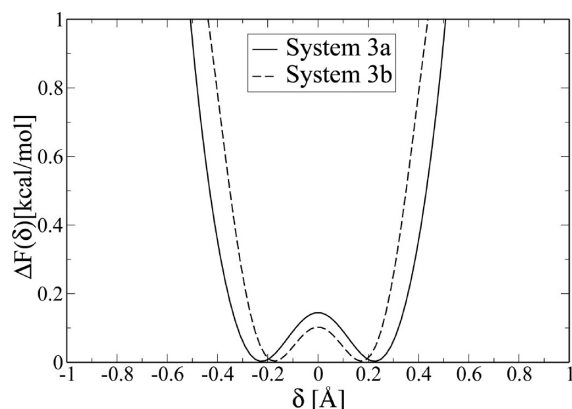


Figure 4. Free energy profiles of PT for hydronium (solid) and hydroxide (dashed) ions in confined 1D water systems with $N = 12$. The reaction coordinate δ is defined in the text.

profiles show that there are small free energy barriers of ~ 0.15 and ~ 0.10 kcal/mol for H^+ and OH^- migration, respectively, in the chain systems, whereas free energy barriers of 0.6 and 1.28 kcal/mol were reported for H^+ and OH^- migration, respectively, in aqueous solutions.^{53,54} Hence, the calculated barrier free energies for the current confined systems are found to be very small compared to those in bulk water. In order to investigate the solvation structure of protonic defects during the PT process, we have calculated the O^*O and O^*H radial distribution functions (RDFs) for both small ($\delta \leq 0.02$ Å) and large ($\delta \geq 0.2$ Å) values of the reaction coordinate. We note that the small value of δ corresponds to the barrier top region (i.e., PT is about to occur), while the large value of δ corresponds to a stable solvated state of the excess proton or the OH^- ion in its “reactant” configuration.

In Figure 5 (panels a and b), we have shown the O^*O and O^*H RDFs for the excess proton system ($N = 12$) for two different values of δ . For the O^*O distribution function, a single peak at ~ 2.45 Å is found for both small and large values of δ which shows that the oxygen–oxygen separation remains essentially constant. However, O^*H distribution shows a splitting of the first peak for the two δ values. We observe three peaks for the small value of δ : the first peak at 0.98 Å for the free or dangling OH bond distance, the second peak at 1.05 Å for one of the hydrogen-bonded OH bond distances, and the third one at 1.21 Å for the hydrogen-bonded OH bond whose hydrogen is also equally shared with a neighboring water ($H_2O \cdots H \cdots OH_2$). For the large value of δ , one sharp peak at 0.98 Å and another broad peak at 1.13 Å with a prominent shoulder at 1.05 Å are found, which correspond to the free and hydrogen-bonded OH bond distances, respectively. The shoulder at 1.05 Å is transformed to a distinct peak and the peak at 1.13 Å gets shifted to 1.21 Å when δ is decreased to a small value of less than 0.02 Å. It may be noted that the O^*H distance of 1.21 Å and O^*O distance of 2.45 Å correspond to an essentially ideal Zundel complex, whereas the O^*H distance of 1.13 Å and O^*O distance of 2.45 Å correspond to a distorted Zundel complex in agreement with the MS-EVB results of ref 37.

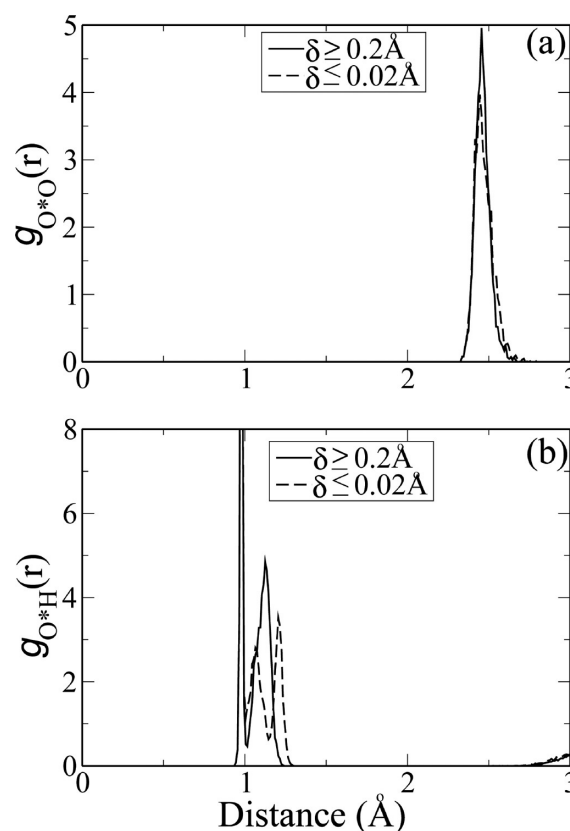


Figure 5. (a) O^*O and (b) O^*H radial distribution functions for the system of an excess proton in a confined water chain ($N = 12$) where O^* is the hydronium oxygen. The solid and dashed curves are for $|\delta| \geq 0.2$ Å and $|\delta| \leq 0.02$ Å, respectively.

Figure 6 (panels a and b) shows the solvation structure of the OH^- ion in the confined system ($N = 12$) through O^*O and O^*H correlations. A sharp major peak around 2.48–2.50 Å is found in the O^*O RDF for both small and large values of δ . Hence, here also, the oxygen–oxygen distance remains essentially unchanged during PT events. The O^*H correlations reveal that the free hydroxyl hydrogen is located 0.98 Å from the oxygen of the OH^- ion for both values of δ . The oxygen of this ion accepts two hydrogen bonds. For the small value of δ , the O^*H distribution shows a second peak at 1.25 Å and a broad third peak around 1.6 Å. The dominant peak at 1.25 Å corresponds to the configuration where the migrating proton is shared nearly equally between the two oxygen atoms ($H-O \cdots H \cdots O-H$). The broad peak at a longer distance is due to the other accepted hydrogen-bond distance of the hydroxide ion. For the large value of δ , two accepted hydrogen-bond distances are seen with a broad peak at 1.4 Å. These results show that no change in the oxygen–oxygen distance or no breaking of a hydrogen bond is required for PT through an ordered 1D chain. This is found to hold for both cases of an excess proton and a hydroxide ion, and hence, PT rates of these systems are expected to be faster than those in bulk water where breaking of a hydrogen bond is required as a prerequisite to PT. In Section 4.2, we present a detailed analysis of the PT rates and quantitative results of the corresponding rate constants.

4.2. Dynamical Properties of Protonic Defects. Proton-transfer (PT) dynamics through 1D water chains are calculated by using the so-called population time-correlation-function

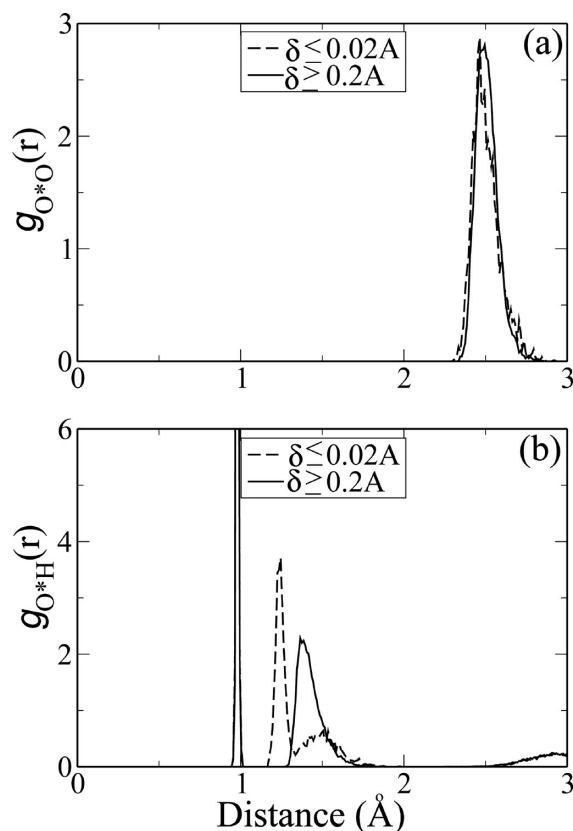


Figure 6. (a) O*O and (b) O*H radial distribution functions for the system of a hydroxide ion in a confined water chain ($N = 12$) where O* is the hydroxyl oxygen. The solid and dashed curves are for $|\delta| \geq 0.2$ Å and $|\delta| \leq 0.02$ Å, respectively.

approach.^{49,55} We define two population variables of PT events, $h(t)$ and $H(t)$, where $h(t)$ is unity when an O* has the same identity at time t as at time $t = 0$ and zero otherwise, and $H(t)$ is unity if O* retains the same identity continuously up to time t from $t = 0$ and zero otherwise. We calculate the continuous PT correlation function defined as^{49,55} $C_c^{O^*O}(t) = \langle h(0)H(t) \rangle / \langle h \rangle$. Since $C_c^{O^*O}(t)$ does not allow any identity change of the charge defect in the interim period, it describes the probability of finding the same O* continuously up to time t . The associated integrated relaxation time (τ_{exch}) can be interpreted as the time needed for O* to change its identity due to PT. Thus, τ_{exch} represents the average timescale of PT events, and its inverse corresponds to the average PT rate. In the calculation of the continuous PT functions, the proton rattling events in which the defect returns to its original O* site after two successive PT events can be either included or excluded. However, these rattling events do not contribute to the overall net displacement of the protonic defects. By including rattling effects, we can calculate the rattling timescales from the short time dynamics of the correlation function, whereas exclusion of such rattling events provides true PT timescales.

An alternative way to study the rate of proton translocation is to calculate the intermittent PT correlation function $C_i^{O^*O}(t) = \langle h(0)h(t) \rangle / \langle h \rangle$ which gives the probability of finding the same O* at time $t = 0$ and time t , irrespective of any possible identity change in the interim period. In the hydrogen-bonded network, both forward and backward PT reactions can take place. In order to determine the rate constant of forward and backward reactions, we define another population variable, $g(t)$, where

$g(t) = 1$ if an oxygen atom which was O* at time $t = 0$ remains either as O* or is found in the first hydration shell of O* at time t ; otherwise, $g(t) = 0$. The projected correlation function $C_n^{O^*O}(t) = \langle h(0)[1 - h(t)]g(t) \rangle / \langle h \rangle$ describes the probability of finding a water molecule in the hydration shell of the hydronium or the hydroxide O* at time t , given that it was itself the O* at time $t = 0$. Including the reverse reaction, we can write the following rate equation for a PT reaction^{49,55}

$$\frac{dC_i^{O^*O}(t)}{dt} = -k_1^{\text{PT}} C_i^{O^*O}(t) + k_{-1}^{\text{PT}} C_n^{O^*O}(t) \quad (4)$$

where k_1^{PT} and k_{-1}^{PT} are the forward and reverse rate constants, respectively. The inverse of the forward rate constant $1/k_1^{\text{PT}}$ corresponds to the average lifetime of a given protonic defect before it gets converted to a water due to a PT event, and it can be compared with τ_{exch} obtained from the route of a continuous correlation function.

We first discuss the results of the continuous correlations including rattling effects. The decays of the continuous time-correlation functions of the hydronium and hydroxide ions, including rattling effects, are shown in Figure 7. The values of

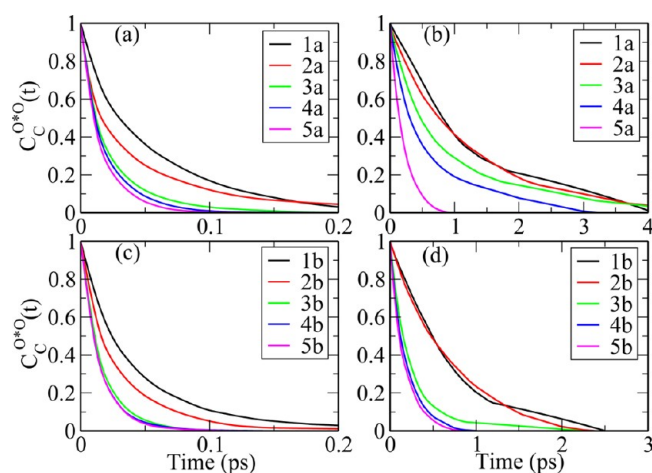


Figure 7. Time dependence of the continuous correlation functions of PT dynamics for hydronium (a and b) and hydroxide (c and d) ions in 1D water chains of varying length. The rattling effects are included in panels a and c, and such effects are excluded in the calculations of the correlation functions shown in panels b and d. Details of various systems are available in Table 1.

the corresponding integrated lifetime (τ_{exch}) are included in Table 2 for both H^+ and OH^- systems. The average lifetime (τ_{exch}) of the hydronium ion decreases with increasing chain length. For $N = 6$, our CPMD and QM/MM simulations predict values of 0.053 and 0.050 ps, respectively, for the case of an excess proton. For the corresponding systems containing OH^- , these values become 0.044 and 0.04 ps for the CPMD and QM/MM simulations, respectively. Hence, the calculated timescales are found to be very similar for the two simulation methods used in the current work. Our QM/MM simulations of longer chain lengths reveal a decreasing trend of the PT timescale with increasing chain lengths for both H^+ and OH^- systems, as can be seen from Table 2. Interestingly, in the present study, the PT rates for OH^- systems are found to be slightly faster than those of the corresponding systems with an excess proton.

Table 2. Timescales of PT Events along 1D Water Chains^a

system	N	H ⁺ / OH ⁻ / H ₂ O	τ_{exch} (ps) (rattling included)	$1/k_1^{\text{PT}}$ (ps) (rattling included)	τ_{exch} (ps) (rattling excluded)	$1/k_1^{\text{PT}}$ (ps) (rattling excluded)
1a	6	H ⁺ / H ₂ O	0.053	0.058	1.234	1.301
1b	6	OH ⁻ / H ₂ O	0.044	0.037	0.674	0.909
2a	6	H ⁺ / H ₂ O	0.050	0.047	1.181	1.408
2b	6	OH ⁻ / H ₂ O	0.039	0.030	0.666	0.714
3a	12	H ⁺ / H ₂ O	0.022	0.023	0.941	0.814
3b	12	OH ⁻ / H ₂ O	0.017	0.018	0.468	0.437
4a	18	H ⁺ / H ₂ O	0.019	0.021	0.621	0.481
4b	18	OH ⁻ / H ₂ O	0.016	0.016	0.188	0.192
5a	30	H ⁺ / H ₂ O	0.016	0.019	0.207	0.229
5b	30	OH ⁻ / H ₂ O	0.015	0.016	0.165	0.182

^aThe results of average lifetimes (τ_{exch}) and inverse rate constants ($1/k_1^{\text{PT}}$) are presented for migration of hydronium and hydroxide ions in water-filled CNTs of varying length.

In order to obtain the rate of PT from intermittent correlations, we have calculated the correlation functions, $C_i^{\text{O}^*\text{O}}(t)$ and $C_n^{\text{O}^*\text{O}}(t)$, directly from the simulation trajectories. For calculation of the correlation function, $C_n^{\text{O}^*\text{O}}(t)$, we have used a cutoff of 3.35 Å for hydration shells of the hydronium and hydroxide ions. The timescales of the inverse forward rate constant ($1/k_1^{\text{PT}}$), which correspond to the average lifetimes of hydronium and hydroxide ions, are also included in Table 2 for all systems. The timescales for both hydronium and hydroxide ions are found to decrease with increasing chain length, which is in agreement with the results of continuous correlations. Generally, the values of $1/k_1^{\text{PT}}$ are found to be comparable with the timescales of τ_{exch} obtained from the route of continuous correlations. Also, similar to our findings from continuous correlations, the inverse rate constants ($1/k_1^{\text{PT}}$) for the excess proton are found to be slightly higher than that of the hydroxide ion for a given chain length. That is, the rate of PT through 1D water chains can be faster for the OH⁻ ion than for that containing an excess proton, contrary to the corresponding PT rates in bulk liquid water.⁵⁵

Next, the rattling events are filtered out because they do not contribute to the net charge displacement along the chains. The decays of the continuous time-correlation functions of the hydronium and hydroxide ions excluding rattling effects are also shown in Figure 7, and the corresponding results of the average lifetimes (τ_{exch}) are included in Table 2. The intermittent correlation functions are also calculated without rattling events, and the corresponding inverse rate constants ($1/k_1^{\text{PT}}$) are also included in Table 2. The average lifetime of the hydronium ion from continuous correlation functions is found to be 1.23 ps from CPMD simulations ($N = 6$), and it becomes 1.18 ps when the same system is studied by the QM/MM method, again showing the similarity of the results obtained from the two simulation methods. Interestingly, even when rattling effects are excluded, PT in OH⁻/H₂O chain systems is found to occur at a somewhat faster rate than that in the corresponding H⁺/H₂O system of equal chain length. Thus, 1D water chains in CNTs

are found to provide highly favorable paths for structural diffusion of OH⁻, so much that it now moves faster than an excess proton. This is also consistent with the free energy profiles of Figure 4 which show a lower barrier for OH⁻ migration than that for an excess proton along a 1D water chain.

The average lifetimes of both hydronium and hydroxide ions are found to decrease gradually with increasing the chain length from $N = 6$ to 12, 18, and 30. Such an increase in the rate of PT with increasing chain length was also found earlier in an empirical valence-bond (EVB) model-based study of proton transport through water-filled CNTs.³⁵ In the present study, it is found that the rates are essentially converged with respect to chain length when rattling effects are included. This is clear from Figure 7(panels a and c) and also Table 2. For example, including rattling effects for the H₃O⁺ systems, the value of $\tau_{\text{exch}}(1/k_1^{\text{PT}})$ changes from 0.019 (0.021) to 0.016 (0.019) ps when the chain length increases from $N = 18$ to $N = 30$. The corresponding timescale for the OH⁻ systems changes from 0.016 (0.016) to 0.015 (0.016) ps for an identical increase in the chain length. The convergence of the PT rates with chain length is found to be somewhat slower when rattling effects are excluded. This is likely due to the fact that the overall dynamics become slower by an order of magnitude when rattling contributions are not counted as PT events. Still, even when rattling effects are excluded, the PT rates for OH⁻ nearly converge. For example, the $\tau_{\text{exch}}(1/k_1^{\text{PT}})$ for OH⁻ systems changes from 0.188 (0.192) to 0.165 (0.182) ps when the chain length is increased from $N = 18$ to 30. For H₃O⁺ systems, the convergence is somewhat slower, which likely arises from the relatively slower rate of PT for H₃O⁺ as compared to that for OH⁻ through 1D water chains.

4.3. Diffusion of Protonic Defects and Water Molecules. The diffusion coefficients of the protonic defects and water molecules are calculated from the mean square displacement (MSD) of the species along the axis (z) of carbon nanotubes. For 1D motion along the z -direction, the MSD is related to the diffusion coefficient by the relation

$$D = \frac{1}{2} \lim_{t \rightarrow \infty} \frac{\langle |z(t) - z(0)|^2 \rangle}{\Delta t} \quad (5)$$

where $z(t)$ is the position vector at time t . We have calculated the diffusion coefficients directly from the slope of the MSD versus time plot. MSDs of three different 1D systems of same length ($N = 12$) containing only water molecules, an excess proton plus water, and a hydroxide ion plus water are calculated to compare the 1D diffusion of protonic defects with that of water (results not shown here). The diffusion coefficient of water through the 1D chain is found to be $0.16 \text{ Å}^2 \text{ s}^{-1}$, whereas values of 2.8 and $3.3 \text{ Å}^2 \text{ s}^{-1}$ are found for the diffusion coefficients of the hydronium and hydroxide ions, respectively. Clearly, the calculated diffusion coefficients of the hydronium and hydroxide ions in these 1D water systems are much higher than those of water molecules themselves due to fast PT events. We note that the current diffusion coefficient of the hydronium ion compares well with the value of $4.0 \text{ Å}^2 \text{ s}^{-1}$ obtained in a previous empirical valence-bond (EVB) model-based study³⁵ for the same chain length. The results are in the same ballpark, considering the fact that the calculations of interaction potentials and run lengths of the two simulations are quite different. The current diffusion-coefficient values also show that the hydroxide ion moves slightly faster than the hydronium ion through 1D water chains. Similar behavior has also been found

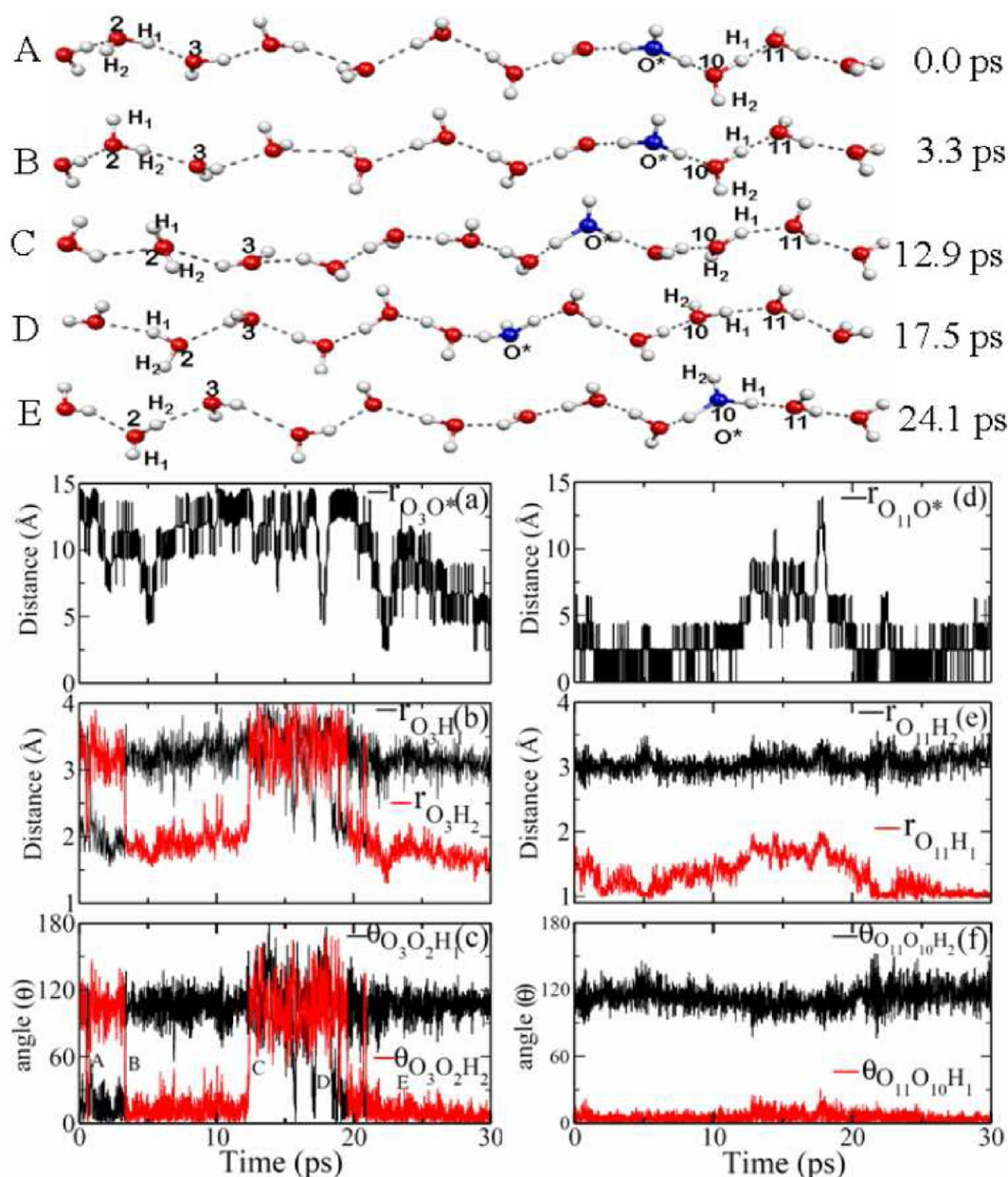


Figure 8. Snapshots taken from our simulation of an excess proton in water chain ($N = 12$) at different time steps. The hydronium oxygen is shown in blue (CNT is not shown here). The movements of the D defect and the excess proton are shown (top). The bottom shows the changes of intermolecular distances and angles in the vicinity of the D defect (left) and the excess proton (right).

for other chain lengths. For example, the calculated diffusion coefficients of H_3O^+ and OH^- for $N = 6$ (18) systems are found to be 1.8 (3.1) and 2.6 (3.5), respectively. This behavior may be contrasted with that in liquid water where hydronium ions are known to move faster than the hydroxide ions.⁸⁰

4.4. Mechanism of Structural Diffusion in 1D Chains.

The excess proton and hydroxide ion mobilities through 1D water chains are found to be significantly faster than that in bulk water. In these 1D chain systems, the mechanisms of structural diffusion of the two ions are found to be different from that of the bulk. According to the presolvation concept, the proton-receiving species and proton-donating species should have similar solvation patterns for a PT to occur. As we have discussed in the previous sections, the solvation structures of the hydronium and hydroxide ions and also of water molecules are different under confinement inside CNTs

compared to those in the bulk. In CNTs with 1D water chains, each water molecule donates one hydrogen bond through one of its hydrogens and accepts one through its oxygen. In such narrow environments, the excess proton is solvated either in a distorted Zundel complex (large value of δ) or as an equally shared ideal Zundel complex, H_5O_2^+ (small value of δ). In both the complexes, the O^*O distance is found to be almost constant (~ 2.45 Å), and the PT barrier is also very small. So, a thermal fluctuation can produce PT events, i.e., a proton can easily get transferred from one oxygen to another oxygen without having to break any hydrogen bond.

In 1D water chains, the hydroxide ion prefers to stay either as a two-coordinated H_5O_3^- complex (large value of δ) with two acceptor hydrogen bonds from two neighboring water molecules or in an equally shared proton complex, H_3O_2^- . Here also, the O^*O distance is found to be almost constant

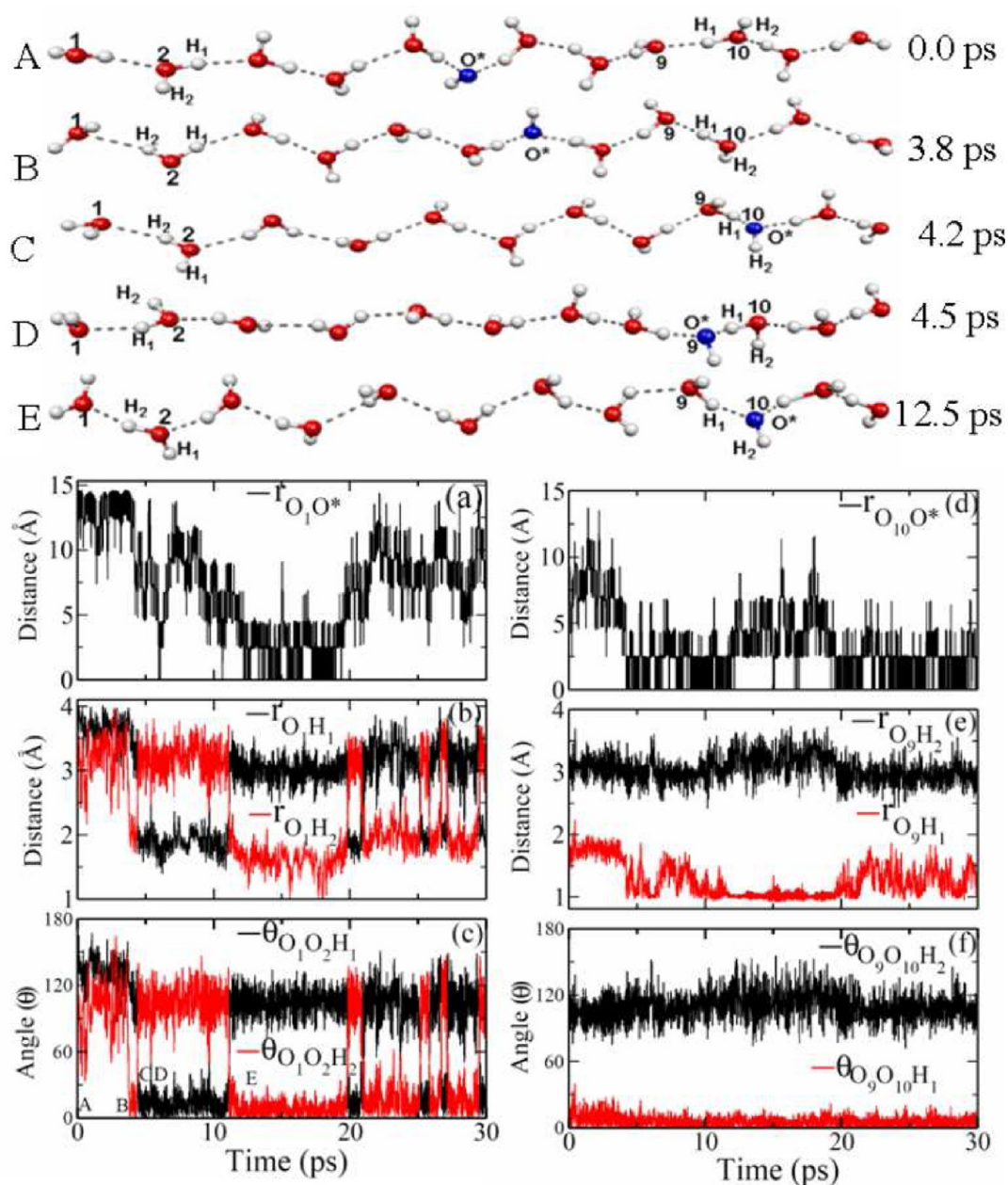


Figure 9. Snapshots taken from our simulation of a hydroxide ion in water chain ($N = 12$) at different time steps. The hydroxide oxygen is shown in blue (CNT not shown). The movements of the L defect and the hydroxide ion are shown in the upper panel. The lower panel shows the changes of intermolecular distances and angles in the vicinity of the L defect (left) and the hydroxide ion (right).

(2.48–2.50 Å). Here, with two acceptor hydrogen bonds, OH^- is nicely presolvated to take a proton from one of its neighboring water molecules. The water itself is also in the right kind of coordination to donate a proton. Thus, here again, PT occurs rather easily without requiring a hydrogen bond to break. It is seen that, for both H^+ or OH^- migration through 1D water chains, both protonic defects and water molecules in their neighborhood are nicely presolvated, and no structural rearrangements or hydrogen-bond fluctuations are required as prerequisites for PT. In the bulk water system, a water–water hydrogen bond needs to be broken for the migration of H^+ , while an acceptor hydrogen bond of a hydroxide ion has to be broken in the OH^- migration process. Breaking of hydrogen bonds has been shown to be the rate-limiting step for proton migration in liquid water.^{50,53,54} Since hydroxide ion–water

hydrogen bonds are stronger and have longer lifetimes than water–water hydrogen bonds,⁵⁵ migration of OH^- does not occur as fast as H_3O^+ in liquid water. However, for the 1D chain systems studied here, a proton can migrate from one oxygen to another oxygen without any hydrogen-bond breaking, and this leads to very fast migration kinetics for both OH^- and H_3O^+ . The OH^- , being smaller and linear, can rotate more easily within the nanotubes to adjust to required orientations. Also, the inherent proton accepting affinity of OH^- is higher than that of H_2O ,⁸¹ and the combined effects of all these factors lead to a slightly faster structural diffusion of OH^- than an excess proton along 1D water chains in confinement.

In Section 3.3, we have shown that water molecules perform angular jumps in the present 1D systems, where free and

hydrogen-bonded hydrogens of a water molecule exchange their hydrogen-bonding states. Therefore, an important issue is whether the 1D PT process involves angular jumps of water molecules. In order to address this issue, we have calculated various intermolecular distances and angles from our simulation trajectories. In Figure 8 (upper panel), we show some snapshots from our excess-proton-in-water-chain ($N = 12$) simulation at different time steps which show movement of the D defect and the excess proton. We see that water molecules perform angular jumps; however, as can be seen from the lower panel of Figure 8, major changes in intermolecular oxygen–hydrogen distances and angles occur due to movement of the D defect. We do not observe any significant jumps of distances and angles in Figure 8 (lower right panel) at the sites of PTs. Our computed $r_{\text{O}_{11}\text{O}^*}$ distance is found to be zero when O_{11} becomes O^* . When O_{11} accepts the excess proton, the $r_{\text{O}_{11}\text{O}^*}$ distance goes to zero, and one hydrogen-bonded hydrogen (H_1 of water O_{10}) comes closer to the O_{11} . During this process, the $r_{\text{O}_{11}\text{H}_1}$ distance decreases from ~ 1.5 to ~ 1.1 Å. So, we can conclude that large-amplitude distance and angular changes are required for D defect migration (i.e., breaking and re-forming of hydrogen bonds need to occur for the movement of D defects), whereas the excess proton can move from one water to another without any hydrogen-bond breaking and angular-jump events.

Similar calculations are also performed for the hydroxide ion systems and are shown in Figure 9. In the upper panel of the figure, we show snapshots from our hydroxide-ion-in-water-chain ($N = 12$) simulation, and our calculated various intermolecular distances and angles are shown in the lower panel. Here also, we do not observe any jumplike changes in the distances and angles (lower right panel) at the sites of OH^- migration through PT. However, such sudden changes in the distances and angles are observed (lower left panel) for migration of the L defect as its movement requires the breaking and formation of hydrogen bonds. In Section 4.5, we present a detailed analysis of the dynamics of these D and L defects.

4.5. Dynamics of D and L Defects. In the present simulations, D defects were found in the excess proton systems while L defects appeared in the water chains containing the OH^- ion. The excess proton and the hydroxide ion interact with these defects which cause a slowing down of the corresponding PT rates. For each of the present systems, we have calculated the probability distribution of the distance between the protonic and the D/L defects, and the results are shown in Figure 10. It is seen that the probability of finding the hydrogen-bonding defects is maximum at half box length distance, which happens to be the largest possible distance in our simulation systems. Thus, the protonic and hydrogen-bonding defects effectively repel each other, and the protonic defects prefer to stay away from the hydrogen-bonding defects as much as possible. For smaller systems ($N = 6$), the hydrogen-bonding defects are present in the second and third solvation shells of the protonic defects. With an increase of the chain length, the D or L defects are found to stay farther from the protonic defects which diminish their retarding effects on PT rates. Hence, an enhancement of the PT rates has been found with increasing chain lengths.

The dynamics of D and L defects in the 1D chain systems are investigated by using a population-correlation-function approach similar to the one used for PT dynamics, except that now O^* represents the oxygen of a D or L defect. We have calculated the continuous correlation functions which describe

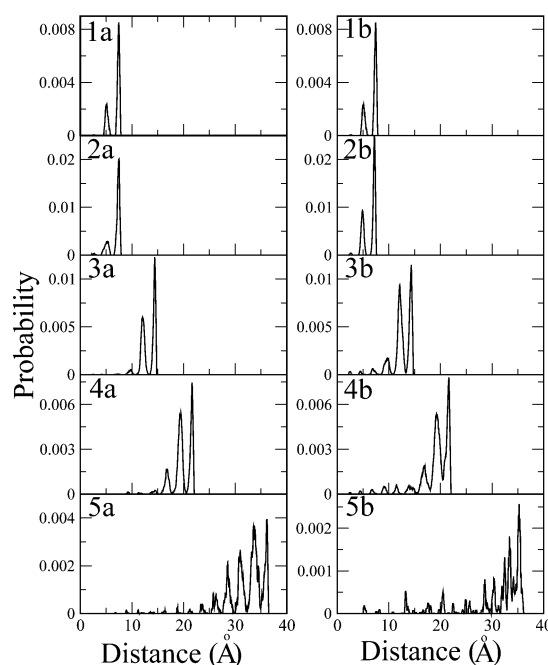


Figure 10. Distributions of the distance between the hydronium oxygen and D defect (left) and the hydroxide oxygen and L defect (right) for water chains of different lengths.

the probability of continuously finding the same O^* for a D or L defect from time $t = 0$ to t (results not shown here). The integrals of the correlation functions for D and L defects, denoted as τ^{D} and τ^{L} , respectively, can be interpreted as the average times needed for D and L defects to change the identity of their oxygens. Hence, τ^{D} and τ^{L} represent the average lifetimes of D and L defects, respectively. The inverses of these timescales correspond to the average rates of defect migration along the water chains. Our calculated values of τ^{D} and τ^{L} are included in Table 3. The lifetime of D defects is found to be

Table 3. Average Lifetimes (τ^{D} and τ^{L}) of D and L Defects from Their Continuous Correlation Functions

system	N	$\text{H}^+/\text{OH}^-/\text{H}_2\text{O}$	τ^{D} (ps)	τ^{L} (ps)
1a	6	$\text{H}^+/\text{H}_2\text{O}$	1.85	
1b	6	$\text{OH}^-/\text{H}_2\text{O}$		1.76
2a	6	$\text{H}^+/\text{H}_2\text{O}$	1.65	
2b	6	$\text{OH}^-/\text{H}_2\text{O}$		1.57
3a	12	$\text{H}^+/\text{H}_2\text{O}$	1.46	
3b	12	$\text{OH}^-/\text{H}_2\text{O}$		1.25
4a	18	$\text{H}^+/\text{H}_2\text{O}$	1.27	
4b	18	$\text{OH}^-/\text{H}_2\text{O}$		1.06
5a	30	$\text{H}^+/\text{H}_2\text{O}$	0.89	
5b	30	$\text{OH}^-/\text{H}_2\text{O}$		0.84

1.85–0.9 ps depending on the chain length, whereas the lifetime of L defects is found to be 1.75–0.85 ps. Generally, like the lifetimes of hydronium and hydroxide ions, the lifetimes of D and L defects are also found to decrease with an increase of chain length. As the chain length is increased, the repulsive potential of interaction between the protonic (hydronium/hydroxide) and D/L defects gets reduced as the average distance between them increases. Also, the stiffness of the repulsive potential is reduced,³⁵ and the D/L defects have more room along the chain to move around for longer chains. Thus,

the retarding effect on the dynamics of D/L defects due to their repulsion with protonic defects is diminished with increasing chain length, and as a result, the D/L defects can move more easily as the chain length is increased. Hence, a decrease in the lifetimes of D and L defects at a given site is observed with increasing chain length. Also, for a given chain length, the average lifetimes of D and L defects are found to be significantly longer than those of the protonic defects (H_3O^+ or OH^-). We note that the D and L defects move along the water chains through rotational and hydrogen-bond reorganizations while protonic defects move through a PT mechanism. Hence, the migration kinetics of D and L defects are found to be slower than those of H_3O^+ and OH^- ions along 1D water chains in CNTs. The slower dynamics of D and L defects are also likely responsible for a slower convergence of the dynamics of these defects as compared to those of PT events on an increase of chain length. It may be noted that the current results of rates of PT along the water chains are nearly converged with respect to chain length, especially when the rattling effects are included.

5. H^+ AND OH^- MIGRATION IN ISOLATED SYSTEMS

We have seen that the presence of D/L defects, which are created at the boundaries due to imposition of periodic boundary condition, reduces the migration rates of H^+ and OH^- ions. Therefore, it would be interesting to see how fast these ions can move through the chain and their relative mobilities in the absence of such D/L defects. To achieve this, we have studied the PT reactions in isolated confined water-chain systems by using the QM/MM simulation method. First, the two protonic defects (hydronium and hydroxide ions) are created at the two ends by adding a proton to and removing a proton from the terminal waters of the $N = 12$ chain system. The system is then equilibrated for about 10 ps, and during this period we fixed the positions of protonic defects to avoid the PT during equilibration. This was achieved by fixing the positions of hydrogens of the hydronium ion and oxygen of the neighboring water and similarly the positions of oxygen of the hydroxide ion and hydrogens of the neighboring water. We continued the simulation run for another 20 ps to create different initial configurations for the study of H^+ and OH^- migration under the influence of opposite charges at the other end. Next, we allow the movement of the protonic defect from one end, while the oppositely charged ion is kept fixed at the other end. The hydronium ion moves from the left end to the right when the hydroxide ion is kept fixed at the right end (Figure 11, top panel). Similarly, the hydroxide ion moves from the right end toward the hydronium ion which is kept fixed at the left end (Figure 11, bottom panel). We have carried out 10 such simulations from different initial configurations for each protonic defect system. Average times taken by the hydronium and hydroxide ions to move from one end to the other are found to be 1.2 and 0.87 ps, respectively. Again, we observe a faster migration of the hydroxide ion than that of the excess proton, which is in agreement with the results of the periodic systems discussed in Section 4.

6. CONCLUSIONS

In this paper, we have presented ab initio molecular dynamics and combined quantum-classical simulations of solvation and migration of an excess proton and of a hydroxide ion along 1D chains of water molecules confined in narrow carbon nanotubes

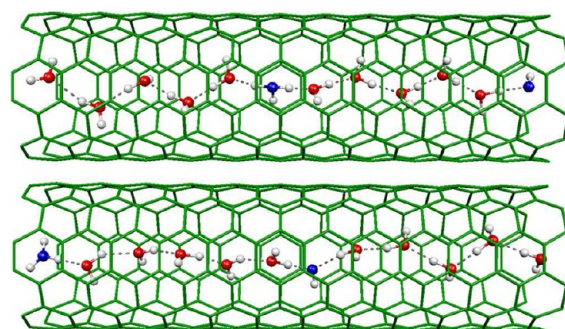


Figure 11. Snapshots taken from our simulations for PT events through water chain ($N = 12$) in the presence of a counterion. The top shows a snapshot of an excess proton moving from the left end to the right when a hydroxide ion is kept fixed at the right end. The bottom shows a snapshot of a hydroxide ion moving from the right end toward the left when the hydronium ion is kept fixed at the left end. The hydronium and hydroxyl oxygens are shown in blue.

(CNT) of varying length. We have also investigated various structural and dynamic properties of pure water inside such narrow pores without any such protonic defects. Our simulations reveal that water molecules are in a single-file arrangement with the average angle of the dipole vector of a molecule with the nanotube axis at about 35° . We found that the rotational relaxation of the dipole vectors of confined water molecules has one faster timescale and another much slower timescale. The hydrogen-bond dynamics of water in these 1D chain systems is also found to be rather slow due to a more rigid hydrogen-bonded environment and less cooperative fluctuations than that in bulk water. The hydrogen-bond breaking and formation events are found to be associated with rotational jumps which also occur much less frequently than that in bulk water.

We have also investigated the rates and mechanisms of PT processes inside the narrow CNTs for cases of both H_3O^+ and OH^- ions. The rates of PT and average lifetimes of these ions are determined by using the so-called population-correlation-function approach. In these water-filled carbon nanotube systems, the water molecules, as well as the hydronium and hydroxide ions, are found to be two-coordinated to donate or accept a proton. No hydrogen-bond breaking is required as a prerequisite for PT in these chain systems, and hence, the rate of PT is found to be rather fast. Our AIMD and QM/MM simulations give similar timescales for PT for a given chain length ($N = 6$). Longer-chain systems are studied by using the QM/MM method only, and from the results of all the systems, we conclude that the hydroxide ion mobility is slightly higher than that of the hydronium ion in these 1D chain systems.

For both the hydronium and hydroxide ion systems, the PT rate increases with the increase in chain length. In our finite-sized simulation systems, two different types of hydrogen-bonding defects (D and L) are found to be formed, which influence the PT rates. D defects are found to arise in the excess proton systems, and L defects are found in the hydroxide ion systems. The protonic defects (H_3O^+ and OH^-) and these orientational hydrogen-bonding defects effectively repel and tend to stay away from each other. These D and L defects are found to move slower than the migration of an excess proton and hydroxide ion; hence, the PT rates can be hindered by the presence of these defects which interrupt the favorable hydrogen-bonded environment for the smooth transfer of a

proton. In systems of increasing chain lengths, the protonic and D/L defects stay farther from each other; hence, protonic defects feel less repelling influence from the D/L defects, and the outcome of this diminishing influence is an increase of the PT rate with increasing chain length. Calculations are also performed for migration of H^+ and OH^- along isolated 1D water chains without any D or L defects. Here also, the migration kinetics of OH^- are found to be little faster than those of an excess H^+ , thus confirming our conclusion that OH^- mobility can be higher than that of an excess proton through 1D water chains in narrow hydrophobic pores. It would be interesting to consider even larger chain lengths to see if the relative rates of migration of hydronium and hydroxide ions, as found in the current systems, still remain for longer chains. Work in this direction is in progress.

AUTHOR INFORMATION

Corresponding Author

*E-mail: amalen@iitk.ac.in.

Present Address

[†]Department of Chemistry, Institute for Computational Molecular Science, Temple University, Philadelphia, PA 19122.

Notes

The authors declare no competing financial interest.

ACKNOWLEDGMENTS

We thank N. Nair for his help in setting up the QM/MM calculations at the initial stage of this work. We also thank Prabal Maiti for many helpful discussions. We gratefully acknowledge financial support from the Board of Research in Nuclear Sciences (BRNS) and the Department of Science and Technology (DST), Government of India.

REFERENCES

- Rasaiah, J. C.; Garde, S.; Hummer, G. *Annu. Rev. Phys. Chem.* **2008**, *59*, 713–740.
- Hummer, G. *Mol. Phys.* **2007**, *105*, 201–207.
- Fang, H.; Wan, R.; Gong, X.; Lu, H.; Li, S. *J. Phys. D: Appl. Phys.* **2008**, *41*, 103002–103017.
- Hille, B. *Ionic Channels of Excitable Membranes*; Sinauer: Sunderland, MA, 1984.
- Ball, P. *Chem. Rev.* **2008**, *108*, 74–108.
- Swanson, J. M. J.; Maupin, C. M.; Chen, H.; Petersen, M. K.; Xu, J.; Wu, Y.; Voth, G. A. *J. Phys. Chem. B* **2007**, *111*, 4300–4314.
- Wikström, M. *Curr. Opin. Struct. Biol.* **1998**, *8*, 480–488.
- Stowell, M. H. B.; McPhillips, T. M.; Rees, D. C.; Soltis, S. M.; Abresch, E.; Feher, G. *Science* **1997**, *276*, 812–816.
- Kreuer, K.-D. *Chem. Mater.* **1996**, *8*, 610–641.
- Gogotsi, Y.; Libera, J.; Yazicioglu, A. G.; Megaridis, C. M. *Appl. Phys. Lett.* **2001**, *79*, 1021–1023.
- Ugarte, D.; Châtelain, A.; de Heer, W. A. *Science* **1996**, *274*, 1897–1899.
- Tsang, S. C.; Chen, Y. K.; Harris, P. J. F.; Green, M. L. H. *Nature* **1994**, *372*, 159–162.
- Dujardin, E.; Ebbesen, T. W.; Hiura, H.; Tanigaki, K. *Science* **1994**, *265*, 1850–1852.
- Ugarte, D.; Stöckli, T.; Bonard, J. M.; Châtelain, A.; de Heer, W. A. *Appl. Phys. A: Mater. Sci. Process.* **1998**, *67*, 101–105.
- Ghosh, S.; Ramanathan, K. V.; Sood, A. K. *Europhys. Lett.* **2004**, *65*, 678–684.
- Maniwa, Y.; Kataura, H.; Abe, M.; Suzuki, S.; Achiba, Y.; Kira, H.; Matsuda, K. *J. Phys. Soc. Jpn.* **2002**, *71*, 2863–2866.
- Byl, O.; Liu, J.-C.; Wang, Y.; Yim, W.-L.; Johnson, J. K.; Yates, J. T. *J. Am. Chem. Soc.* **2006**, *128*, 12090–12097.
- Kolesnikov, A. I.; Zanotti, J.-M.; Loong, C.-K.; Thiyagarajan, P.; Moravsky, A. P.; Loutfy, R. O.; Burnham, C. J. *Phys. Rev. Lett.* **2004**, *93*, 035503–035506.
- Holt, J. K.; Park, H. G.; Wang, Y.; Stadermann, M.; Artyukhin, A. B.; Grigoropoulos, C. P.; Noy, A.; Bakajin, O. *Science* **2006**, *312*, 1034–1037.
- Hummer, G.; Rasaiah, J. C.; Noworyta, J. P. *Nature* **2001**, *414*, 188–190.
- Kofinger, J.; Hummer, G.; Dellago, C. *Proc. Natl. Acad. Sci. U.S.A.* **2008**, *105*, 13218–13222.
- Berezhkovskii, A.; Hummer, G. *Phys. Rev. Lett.* **2002**, *89*, 064503–064506.
- Hanasaki, I.; Nakamura, A.; Yonebayashi, T.; Kawano, S. *J. Phys.: Condens. Matter* **2008**, *20*, 015213–015217.
- Gordillo, M. C.; Marti, J. *Chem. Phys. Lett.* **2000**, *329*, 341–345.
- Mukherjee, B.; Maiti, P. K.; Dasgupta, C.; Sood, A. K. *J. Phys. Chem. B* **2009**, *113*, 10322–10330.
- Zhu, F.; Schulten, K. *Biophys. J.* **2003**, *85*, 236–244.
- Kalra, A.; Garde, S.; Hummer, G. *Proc. Natl. Acad. Sci. U.S.A.* **2003**, *100*, 10175–10180.
- Zimmerli, U.; Gonnet, P. G.; Walther, J. H.; Koumoutsakos, P. *Nano Lett.* **2005**, *5*, 1017–1022.
- Joseph, S.; Aluru, N. R. *Nano Lett.* **2008**, *8*, 452–458.
- Mei, H. S.; Tuckerman, M. E.; Sagnella, D. E.; Klein, M. L. *J. Phys. Chem. B* **1998**, *102*, 10446–10458.
- Vendrell, O.; Meyer, H. J. *Chem. Phys.* **2005**, *122*, 104505–104505.
- Pomés, R.; Roux, B. *J. Phys. Chem.* **1996**, *100*, 2519–2527.
- Pomés, R.; Roux, B. *Chem. Phys. Lett.* **1995**, *234*, 416–424.
- Sadeghi, R. R.; Cheng, H. P. *J. Chem. Phys.* **1999**, *111*, 2086–2094.
- Dellago, C.; Naor, M. M.; Hummer, G. *Phys. Rev. Lett.* **2003**, *90*, 105902–105905.
- Dellago, C.; Hummer, G. *Phys. Rev. Lett.* **2006**, *97*, 245901.
- Cao, Z.; Peng, Y.; Yan, T.; Li, S.; Li, A.; Voth, G. A. *J. Am. Chem. Soc.* **2010**, *132*, 11395–11397.
- Mann, D. J.; Halls, M. D. *Phys. Rev. Lett.* **2003**, *90*, 195503–195506.
- Hassan, S. A.; Hummer, G.; Lee, Y. S. *J. Chem. Phys.* **2006**, *124*, 204510–204518.
- Vaitheeswaran, S.; Rasaiah, J. C.; Hummer, G. *J. Chem. Phys.* **2004**, *121*, 7955–7965.
- Pomés, R.; Roux, B. *Biophys. J.* **1998**, *75*, 33–40.
- Sagnella, D. E.; Laasonen, K.; Klein, M. L. *Biophys. J.* **1996**, *71*, 1172.
- Pomés, R.; Roux, B. *Biophys. J.* **2002**, *82*, 2304–2316.
- Brewer, M. L.; Schmitt, U. W.; Voth, G. A. *Biophys. J.* **2001**, *80*, 1691–1702.
- Habenicht, B. F.; Paddison, S. J.; Tuckerman, M. E. *Phys. Chem. Chem. Phys.* **2010**, *12*, 8728.
- Habenicht, B. F.; Paddison, S. J. *J. Phys. Chem. B* **2011**, *115*, 10826–10835.
- de Grotthuss, C. J. T. *Ann. Chim.* **1806**, *LVIII*, 54.
- Marx, D. *Chem. Phys. Chem.* **2006**, *7*, 1848–1870.
- Marx, D.; Chandra, A.; Tuckerman, M. E. *Chem. Rev.* **2010**, *110*, 2174.
- Tuckerman, M. E.; Chandra, A.; Marx, D. *Acc. Chem. Res.* **2006**, *39*, 151–158.
- Voth, G. A. *Acc. Chem. Res.* **2006**, *39*, 143–150.
- Tuckerman, M. E.; Laasonen, K.; Sprik, M.; Parrinello, M. *J. Chem. Phys.* **1995**, *103*, 150–161.
- Marx, D.; Tuckerman, M. E.; Hutter, J.; Parrinello, M. *Nature* **1999**, *397*, 601604.
- Tuckerman, M. E.; Marx, D.; Parrinello, M. *Nature* **2002**, *417*, 925–929.
- Chandra, A.; Tuckerman, M. E.; Marx, D. *Phys. Rev. Lett.* **2007**, *99*, 145901–145904.
- Agmon, N. *Isr. J. Chem.* **1999**, *39*, 493–502.

- (57) Asthagiri, D.; Pratt, L. R.; Kress, J. D. *Proc. Natl. Acad. Sci. U.S.A.* **2005**, *102*, 6704–6708.
- (58) Car, R.; Parrinello, M. *Phys. Rev. Lett.* **1985**, *55*, 2471–2474.
- (59) Laio, A.; VandeVondele, J.; Roethlisberger, U. *J. Phys. Chem. B* **2002**, *106*, 7300–7307.
- (60) Laio, A.; VandeVondele, J.; Roethlisberger, U. *J. Chem. Phys.* **2002**, *116*, 6941.
- (61) Berendsen, H. J. C.; Grigera, J. R.; Straatsma, T. P. *J. Phys. Chem.* **1987**, *91*, 6269–6271.
- (62) Hutter, J.; Alavi, A.; Deutsch, T.; Bernasconi, M.; Goedecker, S.; Marx, D.; Tuckerman, M. E.; Parrinello, M. *CPMD Program*; MPI für Festkörperforschung and IBM Zurich Research Laboratory: Stuttgart, Germany, and Zurich, Switzerland, 1997–2001, and 1990–2011.
- (63) Kohn, W.; Sham, L. *Phys. Rev. A: At., Mol., Opt. Phys.* **1965**, *140*, 1133–1137.
- (64) Becke, A. D. *Phys. Rev. A: At., Mol., Opt. Phys.* **1988**, *38*, 3098–3100. Lee, C.; Yang, W.; Parr, R. G. *Phys. Rev. B: Condens. Matter Mater. Phys.* **1988**, *37*, 785–789.
- (65) Vanderbilt, D. *Phys. Rev. B: Condens. Matter Mater. Phys.* **1990**, *41*, 7892–7895.
- (66) Nose, S. *J. Chem. Phys.* **1984**, *81*, 511. Hoover, W. G. *Phys. Rev. A: At., Mol., Opt. Phys.* **1985**, *31*, 1695.
- (67) Kuo, I.-F. W.; Mundy, C. J.; McGrath, M. J.; Siepmann, J. I.; VandeVondele, J.; Sprik, M.; Hutter, J.; Chen, B.; Klein, M. L.; Mohamed, F.; Krack, M.; Parrinello, M. *J. Phys. Chem. B* **2004**, *108*, 12990.
- (68) van Gunsteren, W. F.; et al. *Biomolecular Simulation: GROMOS96 Manual and User Guide*; BIOMOS b.v.: Zürich, 1996.
- (69) Cornell, W. D.; Cieplak, P.; Bayly, C. I.; Gould, R. I.; Merz, M. K.; Ferguson, D. M.; Spellmeyer, D. C.; Fox, T.; Caldwell, F. J.; Kollman, P. A. *J. Am. Chem. Soc.* **1995**, *117*, 5179–5197.
- (70) Rapaport, D. C. *Mol. Phys.* **1983**, *50*, 1151–1162.
- (71) Luzar, A.; Chandler, D. *Nature* **1996**, *379*, 55. Luzar, A. *J. Chem. Phys.* **2000**, *113*, 10663.
- (72) Chandra, A. *Phys. Rev. Lett.* **2000**, *85*, 768–771.
- (73) Balasubramanian, S.; Pal, S.; Bagchi, B. *Phys. Rev. Lett.* **2002**, *89*, 115505.
- (74) Mallik, B. S.; Semparathi, A.; Chandra, A. *J. Phys. Chem. A* **2008**, *112*, 5104.
- (75) Chakraborty, D.; Chandra, A. *Chem. Phys.* **2012**, *392*, 96.
- (76) Debye, P. *Polar Molecules*; The Chemical Catalog Company: New York, 1929.
- (77) Laage, D.; Hynes, J. T. *Science* **2006**, *311*, 832–835.
- (78) Jorgensen, W. L.; Chandrasekhar, J.; Madura, J. D.; Impey, R. W.; Klein, M. L. *J. Chem. Phys.* **1983**, *79*, 926–935.
- (79) Mahoney, M. W.; Jorgensen, W. L. *J. Chem. Phys.* **2000**, *112*, 8910–8922.
- (80) Atkins, P.; de Paula, J. *Atkins' Physical Chemistry*, 8th ed.; Oxford University Press: New York, 2006; p 766.
- (81) Jolly, W. L. *Modern Inorganic Chemistry*, 2nd ed.; McGraw-Hill: New York, 1991.